Scientific Research Publishing

Open Journal of Applied Sciences, 2026, 16(8), 2819-2841
https://www.scirp.org/journal/ojapps
ISSN Online: 2165-3925
ISSN Print: 2165-3917

Production and Characterization of Activated Carbon from Soybean Hulls for Methylene Blue Dye Removal: Adsorption Kinetics, Adsorption Isotherms and Intraparticle Diffusion

Sodoadika Akpolou[1*], Samadou Sanni[2], Clément Kolawole Balogoun[3], Ibrahim Tchakala[2], Moursalou Koriko[1], Gado Tchangbedji[1]

[1]Laboratoire de Gestion Traitement et Valorisation des Déchets, Université de Lomé (GTVD/UL), Lomé, Togo
[2]Laboratory of Applied Hydrolgy and Environment, University of Lome (LHAE/UL), Lomé, Togo
[3]Applied Chemistry Study and Research Laboratory, Polytechnic School of Abomey-Calavi, Cotonou, Benin
Email: *sodoadikaa@gmail.com

How to cite this paper: Akpolou, S., Sanni, S., Balogoun, C.K., Tchakala, I., Koriko, M. and Tchangbedji, G. (2026) Production and Characterization of Activated Carbon from Soybean Hulls for Methylene Blue Dye Removal: Adsorption Kinetics, Adsorption Isotherms and Intraparticle Diffusion. *Open Journal of Applied Sciences*, **16**, 2819-2841.
https://doi.org/10.4236/ojapps.2026.168158

Received: July 25, 2026
Accepted: August 24, 2026
Published: August 27, 2026

Abstract

Dyes represent an important category of pollutants that are harmful for aquatic organisms, human health and the environment. The present study aims to prepare activated soybean hulls carbon (ASHC) in order to apply for the removal of methylene blue (MB) dye. To this end, the phosphoric acid chemical method was adopted for the synthesis of activated carbon from soybean hulls. Furthermore, physicochemical and textural characterizations were performed, including analyses by thermogravimetric (TG-DTG) analysis, X-ray diffraction (XRD), scanning electron microscopy (SEM), energy-dispersive X-ray (EDX) spectroscopy, and the Lopez-Ramon method (1999). An experimental study of MB dye removal using the batch method was carried out for ASHC adsorption capacity evaluation. First-order and second-order adsorption kinetics, Langmuir and Freundlich adsorption isotherms, and intraparticle diffusion were determined. Specifically, the mass yield and low ash content, parameters indicating the amorphous state of the adsorbent, and the pH at the zero-charge point (pH_{ZPC}= 4.25) were determined. XRD indicates the absence of crystallization in the activated charcoal. SEM at 25 µm illustrates the picture of the surface of the charcoal. EDX analysis of the activated charcoal reveals the presence of carbon and oxygen. Characterization and experimental results show that the ASHC is amorphous. Experimental adsorption studies reveal an MB removal rate exceeding 96%; the pseudo-first-order kinetic model, the second-order model, and intraparticle diffusion were investigated. ASHC is therefore a potential alternative adsorbent for wastewater

treatment. The results of the adsorption data were better described by pseudo-second order kinetic model. It is revealed that both Langmuir isotherm model and Freundlich isotherm model fit the equilibrium data.

Keywords

Soybean Hulls, Activated Carbon Characterization, Methylene Blue Dye, Adsorption

1. Introduction

In the recent years, the dyes production has increased worldwide because of high demand. There are approximately 10,000 distinct categories of dyes and the global production of dyes is estimated at 7105 tons annually. The textile industry uses synthetic dyes to color various products such as fibers and yarns [1] [2]. These synthetic dyes are non-biodegradable organic compounds with aromatic structures and can cause severe undesirable effects. They are very harmful for the human health due to their toxic, mutagenic, and carcinogenic properties [3] [4]. Wastewater generated by these industries is heavily laden with dyes. This industrial wastewater is often discharged into rivers, streams, lakes, and the environment. The presence of these dyes in surface waters poses a threat to the environment, human health, and aquatic life. Methylene blue (MB), a dye with a stable aromatic structure, can cause gastrointestinal irritation, nausea or vomiting, dyspnea, and cyanosis if ingested [5]. These dyes have the properties to reduce solar infiltration into waters, consequently altering the photosynthesis activity, disrupting aquatic life and degrading water quality [1] [6]. In this context, it is an emergency to propose alternative techniques in order to completely remove dyes from wastewater. Adsorption is the emergent technique among diverse methods due to its advantages. The adsorption is simple in application, ease of operation, low cost process, non-generation of dangerous by-products and is efficient for effluent treatment [7]. For the industries, the low-cost adsorbents such as activated carbon with high adsorption capacities become an interesting option among the conventional adsorbents.

Agricultural activities lead to the production of ever-increasing by-products rich in cellulose, hemicellulose, and lignin. Transforming agri-food residues into activated carbon offers a sustainable, value-added product alternative; it contributes to promoting the circular economy and reducing environmental pollution [8] [9]. Previous studies have addressed the production and uses of activated carbon. Furthermore, activated carbons are adsorbents that find applications in water treatment, gas purification, and dye removal [10] [11]. Various local agricultural residues have been used as precursor materials for activated carbons. For example, cotton residue [12], corn cobs and stalks [13] [14], peanut shells [15], bean husk [16] and coconut shells [17] have been used to

prepare activated carbons using the chemical activation method. In reality, there are two activation modes: chemical activation (400˚C - 700˚C) and physical activation (800˚C - 1000˚C) [18] [19]. The two most commonly used chemical agents are zinc chloride and phosphoric acid. In recent years, phosphoric acid has been used more frequently in the chemical activation of coal, not only for economic and environmental reasons, but also because it contributes to the proliferation of micro- and mesoporosities in the coal matrix [20]. The applications of adsorbents depend on understanding their properties, which are in turn deduced from physicochemical and textural characterizations.

The soybean, *Glycine max,* is cultivated for its protein-rich seeds in various regions (Plateaux, Centrale) of Togo. After harvesting and shelling, the seeds are discarded; they are part of the agricultural residues generated and left behind after harvest. However, soybean hulls contain cellulose (48.1%), hemicellulose (19.7%), lignin (4.3%), protein (11.8%) and low ash (3.7%) [21] [22] and can be used to produce value-added products, such as activated carbon.

The most widespread method for treating soybean by-products remains combustion, which generates harmful gases, contributing to environmental pollution. The preparation of activated carbon requires an economic investment that impacts its use, even though it is effective for water treatment [23]. It is necessary to find simple, local resources to ensure the production of adsorbents at a lower cost. Soybean husks, available locally, are a biomass that can be transformed into activated carbon, as an alternative to commercial activated carbon. Therefore, precursor materials, soybean hulls, were collected from farmers in the Plateaux Region of Togo for processing into activated carbon.

The objective of this study is to prepare activated carbon from soybean hulls and to characterize it using physicochemical and textural methods. Furthermore, the study aims to apply the carbon to the removal of methylene blue dye. The activated carbon is prepared using a chemical activation method with phosphoric acid. Characterization techniques include X-ray diffraction (XRD), thermogravimetric (TG-DTG) analysis, scanning electron microscopy (SEM) coupled with energy-dispersive X-ray spectroscopy (EDX), the Lopez-Ramon method, and ash content determination. First-order and second-order adsorption kinetics, Langmuir and Freundlich adsorption isotherms, and intra-particle diffusion were determined.

2. Materials and Methods

2.1. Materials and Chemicals

The raw materials used for the synthesis of activated carbon are soybean hulls. These precursor materials, soybean hulls, were collected from farmers at the Plateaux Region of Togo. To prepare the activated carbon and perform the physicochemical analyses, the following chemical reagents were used. Phosphoric acid H_3PO_4 (85%) is purchased from Park Scientific Limited, Northampton, UK; hydrochloric acid (ACS, 37%) is from Merk KGaA, Darmstadt Germany, USA; sodium chloride (NaCl, ≥99.5%), sodium hydroxide (NaOH, 98%), methylene blue

(Molecular mass: 319.85 g·mol^{-1}, chemical formula: $C_{16}H_{18}N_3SCl$) are purchased from Sigma Aldrich, St Louis, MO, USA.

2.2. Preparation of Activated Charcoal

The preparation of activated soybean hulls carbon (ASHC) is performed as described Akpolou *et al*. (2026) [24]. The sample was then washed with distilled water to remove impurities and dried at room temperature on a laboratory bench. Using a blender, the hulls were ground into small pieces (1 mm particle size) and then dried again, this time in an oven (ISUZU brand) at 105˚C for 24 hours before impregnation.

After drying, the soybean hulls were impregnated with a dilute H_3PO_4 50% phosphoric acid solution at a ratio of 2:1 ($m_{\text{phosphoric acid}}/m_{\text{precursor}}$). The resulting mixture was thoroughly kneaded using a stick and stored in an airtight container for 24 hours before carbonization.

The impregnate is distributed into pre-dried porcelain crucibles; these are weighed and placed in a container, a metal jar designed and adapted to hold the sample crucibles. The jar containing the samples is placed in the electric furnace (SNOL brand). Carbonization is a pyrolysis process carried out at 400˚C for 2 hours in inert conditions. The temperature rises from ambient to 400˚C at heating rate of 5˚C·min^{-1}, where it stabilizes within a range for 2 hours before decreasing. The carbonized material, activated carbon, is removed from the furnace, placed in a desiccator for cooling, and then weighed before washing. The mass yield of production and the activation rate (burn-off) of activated carbon are determined by (1) and (2).

$$\text{Mass}(\%) = \frac{m_{\text{AC}}}{m_{\text{Precursor}}} \times 100 \tag{1}$$

$$\text{Burn-Off}(\%) = \frac{m_{\text{Precursor}} - m_{\text{AC}}}{m_{\text{Precursor}}} \times 100 \tag{2}$$

The activated carbon is washed first in a hydrochloric acid solution (0.1M) for 24 hours, then thoroughly washed with distilled water until the residual water reaches a constant pH (pH200E meter). After filtration and drying at 105˚C for 24 hours, the activated carbon is stored in a sealed container for characterization.

2.3. Characterization

The activated carbon produced is characterized using physico-chemical and textural analysis techniques, including X-ray diffraction (XRD), scanning electron microscopy (SEM) coupled with energy-dispersive X-ray (EDX) analysis, thermogravimetric analysis, the Lopez-Ramon method (1999), and the ash content determination method.

X-ray diffraction (XRD) techniques performed at angles 2θ ranging from 5˚ to 69.8˚ using a Brucker D8 Advance diffractometer equipped with a copper anode and the ash content determination technique [13] were used to identify the mineralogical composition and crystalline phases present in the coal. Scanning electron microscopy (SEM) coupled with energy-dispersive X-ray spectroscopy (EDX) en-

abled observation of the pore distribution on the surface of the activated carbon and its elemental chemical composition. Thermogravimetric analyses (TGA) were performed to investigate the thermal stability of the prepared activated carbon and to determine the different decomposition phases. The Lopez-Ramon method (1999) [12] was used to determine the pH at the zero-charge point, and the burn-off value was determined to infer the nature of the material's porosity.

Knowledge of these characteristics will not only allow us to evaluate the adsorption capacity of the analyzed activated carbon, but will also guide its application in the context of pollutant removal.

2.4. Mechanism of Adsorption of MB Dye: Experimental Study

To determine the usefulness of activated soybean hulls carbon (ASHC), as an adsorbent, the adsorption of a model dye, methylene blue (MB), was studied. First, 1 $g{\cdot}L^{-1}$ of MB stock solution was prepared by dissolving 1 g of MB powder in the 1000 mL volumetric flask with distilled water. Several daughter solutions were prepared by diluting an appropriate volume of the stock solution, and then calibration was performed. The experimental studies (solution preparation, adsorption, concentration determination) were carried out in laboratory at ambient temperature fixed at 20˚C. The adsorption volume is 200 mL. The contact time of mixture (ASHC + MB) is relative to initial concentration C_0 of MB solution: 27 min, 65 min, 45 min, 55 min respectively for 20 $mg{\cdot}L^{-1}$, 30 $mg{\cdot}L^{-1}$, 40 $mg{\cdot}L^{-1}$, 50 $mg{\cdot}L^{-1}$.

The absorbance of the solutions was read using an Ultraviolet-visible (UV-vis) spectrophotometer (INESA 754N) at a wavelength of λ = 620 nm.

Figure 1 displays calibration curve of methylene blue and correspondent equation applied to calculate the residual concentrations of the MB solutions ($mg{\cdot}L^{-1}$). It is obtained by plotting MB concentration ($mg{\cdot}L^{-1}$) versus the absorbance line by Origin. The MB concentration range for calibration is from 0 to 10 $mg{\cdot}L^{-1}$.

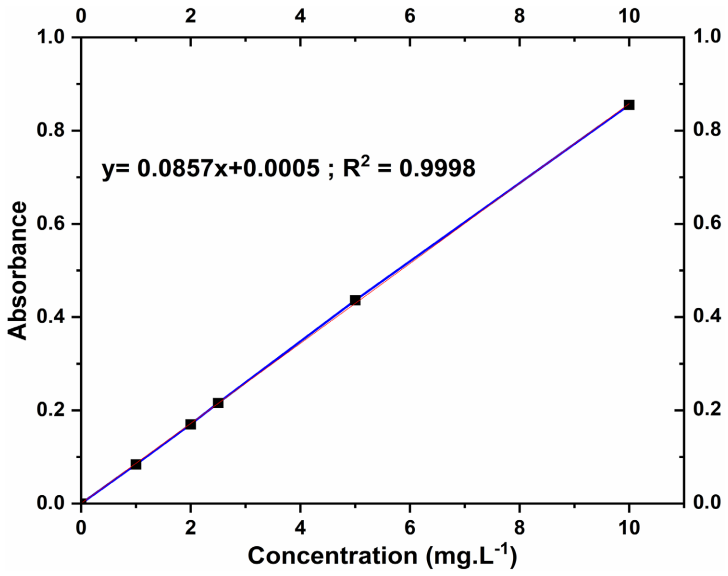

Figure 1. Calibration curve; MB concentration range: from 0 to 10 $mg{\cdot}L^{-1}$.

Experimental studies of MB adsorption on ASHC were conducted by applying a batch method. Some quantity of ASHC was introduced into a 250 mL beaker containing 200 mL of a MB solution of a given initial concentration. The mixture (ASHC + MB) was then subjected to magnetic stirring (using Thermo SCIENTIFIC brand stirrer) at 300 rotations per minute (rpm). At regular intervals, samples were taken, the residual concentrations of MB were determined. Furthermore, the effect of ASHC mass, the effect of solutions pH and the effect of initial concentrations on the equilibrium contact time adsorption were investigated. The initial concentrations of MB solutions (C_0) values such as 20 mg·L^{-1}, 30 mg·L^{-1}, 40 mg·L^{-1}, 50 mg·L^{-1} were used to carry out the adsorption experiment on 0.1 g, 0.2 g, 0.3 g and 0.4 g of ASHC. The influence of pH on MB (30 mg·L^{-1}) were conducted using pH values ranging from 2 to 10. The pH of each solution was adjusted by adding 0.1 mol·L^{-1} HCl or NaOH solutions. Subsequently, 0.1 g of activated carbon was added to 250 mL beakers containing 200 mL of the BM solutions.

The amount of MB adsorbed per unit mass and the percentage of ASHC elimination are determined by using the equations (3) and (4).

$$q\left(\mathrm{mg}\cdot\mathrm{g}^{-1}\right)=\frac{\left(C_0-C_e\right)\times V}{m} \tag{3}$$

$$\mathrm{Removal}\left(\%\right)=\frac{C_0-C_e}{C_0}\times 100 \tag{4}$$

where C_0 and C_e denote the initial concentration of MB and the equilibrium concentration of BM, respectively; m and V represent the mass of ABPC and the adsorption volume, respectively. First-order and second-order kinetic adsorption studies, Langmuir and Freundlich adsorption isotherms, and intraparticle diffusion were explored to explain the interactions between MB molecules and ASHC. To investigate the adsorption mechanism of BM dye onto activated soybean hull carbon (ASHC), it was essential to determine the adsorption kinetics (first-order and second-order), adsorption isotherms (Langmuir and Freundlich models), and intraparticle diffusion.

2.5. Kinetics, Isotherms Adsorption and Intraparticle Diffusion

2.5.1. Adsorption Isotherms

Adsorption isotherms describe the process by which an adsorbate attaches to the surface of an adsorbent at a constant temperature. Furthermore, they serve as indicators to quantify the substances adsorbed onto the solid surface and to deduce the affinity between the adsorbate and the adsorbent.

The Freundlich isotherm assumes that the adsorbent's surface sites are heterogeneous. The linear form of the Freundlich isotherm allows for the determination of the surface heterogeneity intensity and the associated energy distribution.

The Langmuir adsorption isotherm is characterized by plotting the graph of $(\frac{1}{q_e})$ versus $(\frac{1}{C_e})$ whereas the Freundlich adsorption isotherm is obtained from

the plot of $\ln(q_e)$ versus $\ln(C_e)$. If the resulting plot yields a straight line for a given model, that model can describe the dye adsorption process. Equations 5 and 6 represent Langmuir and Freundlich isotherms models respectively [4] [25]-[27].

$$\frac{1}{q_e} = \frac{1}{q_{\max} K_L} \frac{1}{C_e} + \frac{1}{q_{\max}} \tag{5}$$

$$\ln(q_e) = \ln(K_f) + \frac{1}{n} \ln(C_e) \tag{6}$$

K_L (L·mg^{-1}) and $q_{\max}$ (mg·g^{-1}) respectively denote the Langmuir constant and the maximum adsorption capacity; K_L characterizes the interactions between the BM dye and the ASHC; K_L characterizes the strength of an adsorption. The parameters $q_{\max}$, K_L, R_L (L·mg^{-1}), $\frac{1}{n}$, K_f are determined by equations 7, 8, 9, 10 and 11.

$$q_{\max} = \frac{1}{\text{Intercept}} \tag{7}$$

$$K_L = \frac{1}{\text{Slope} \times q_{\max}} \tag{8}$$

$$R_L = \frac{1}{1 + C_i \times K_L} \tag{9}$$

$$\frac{1}{n} = \text{Slope} \tag{10}$$

$$K_f = \text{Antiln}(\text{Intercept}) \tag{11}$$

where C_i (mg·L^{-1}) is initial concentration of adsorption solution. Note that K_f and $\frac{1}{n}$ are Freundlich constants; K_f determines the adsorption capacity and $\frac{1}{n}$ measures the heterogeneity of the adsorption intensity or the degree of non-linearity [3].

2.5.2. Adsorption Kinetics

Adsorption kinetics according to two kinetic models, pseudo-first order and pseudo-second order, were analyzed. The adsorption kinetics of the pseudo-first order and the adsorption kinetics of the pseudo-second order are obtained by plotting the graph of $\ln(q_e - q_t)$ versus time (t) and the graph of $\frac{t}{q_t}$ versus t (time), represented by equations 12 and 13 respectively.

$$\ln(q_e - q_t) = \ln(q_e) - k_1 t \tag{12}$$

$$\frac{t}{q_t} = \frac{1}{k_2 q_e^2} + \frac{1}{q_e} t \tag{13}$$

The rate constants k_1 and k_2 the amount MB adsorbed at equilibrium are determined from the equations of the linear fit lines corresponding to equations 12 and 13.

Pseudo-first-order kinetics assume that the reaction rate is proportional to the concentrations of dyes/pollutants in the solution and is controlled by surface interactions of the adsorbent. However, pseudo-second-order kinetics assume that adsorption is chemical in nature and occurs in determinate steps; it allows us to deduce whether there are interactions between the adsorbate molecules and the adsorbent surface, interactions which will potentially enhance adsorption.

2.5.3. Intraparticle Diffusion

The adsorption of dye can be explained by the intraparticle diffusion model. When adsorption reactions occur via intraparticle diffusion, the curve representing the quantity of dye adsorbed per unit mass of adsorbent (q_t) versus square root of time ($t^{\frac{1}{2}}$) is a straight line, represented by equation 14.

$$q_t = k_d t^{\frac{1}{2}} + C \tag{14}$$

k_d is the intraparticle diffusion constant and C ($mg{\cdot}g^{-1}$) is the constant that characterizes the boundary layer thickness. When the value of the constant C is zero, intraparticle diffusion is the limiting phenomenon of the adsorption process; when it is negative, adsorption is slow; it is fast when C is positive [28].

3. Results and Discussion

3.1. Mass Yield and Activation Rate

The mass yield of activated carbon soybean hulls is 44.85%, and the corresponding activation rate is 55.15%. This high activation rate, or loss on ignition (great than 50%), indicates that the activated carbon will tend to develop medium to large pores (mesopores and macropores). Loss on ignition (burn-off) is due to the loss of volatile matter and particles under the effect of heat during carbonization, ultimately creating pores within the material [12]. The nature of the pores depends on the precursor materials, as well as the preparation conditions.

3.2. The Ash Contents

The ash content of activated carbon is one of parameters used to appreciate his adsorption capacity. In the present investigation, the standard method is applied to determine the ash content of the activated carbon elaborated. In terms of result, the ash content value of is relatively low and equals to 5.59%. This result is characteristic of the amorphous solid, without or very low mineralogical composition. Then, the activated carbon prepared from soybean hulls is amorphous porous solid. Additionally, approximate results have been reported in the literature for activated carbon made from cashew nut shells at 400˚C (5.66%) [29] and activated carbon prepared from the kernel shell of *Balanites aegyptiaca* (6.66%) [30]. Indeed, the high ash content of activated carbons reduces their pollutant adsorption capacity; the minerals constituting the ash obstruct certain pores [31] [32] and prevent access to adsorption sites.

3.3. The pH at the Point of Zero Charge of Activated Carbon

Figure 2(a) shows the result of the pH at the point of zero charge (pH_{PZC}) of activated carbon analyzed by the bisector method. So, the value of pH at point of zero charge (pH_{PZC}) is equal to 4.25.

This may be due to the raw material and the phosphoric acid chemical activation method used during charcoal preparation. Similar results have been reported in some studies in the literature, particularly for activated charcoals obtained by phosphoric acid activation of the kernel shells of *Balanites aegyptiaca (L.) Del. fruits* (pH_{PZC} = 5.08) [31], cottonseed cake (pH_{PZC} = 5.3) [12], and corn cobs (pH_{PZC} = 5.3) [13]. At the point of zero charge, the surface of the carbon carries as many negative charges as positive charges, which neutralize each other. Adsorbents with high values of pH_{PZC} have a great affinity for adsorbing anionic pollutants, while those with low values are more favorable for binding cationic pollutants [33]. If the pH is low ($pH < pH_{PZC}$), there is protonation of the oxygenated sites on the carbon surface, which becomes positively charged, leading to cation repulsion. Thus, the adsorption capacity of the adsorbent for cationic pollutants under this condition is reduced. However, when the pH is high ($pH > pH_{PZC}$), the surface of the adsorbent becomes negatively charged, which is favorable to the adsorption of cations from pollutants through electrical attraction [34].

3.4. X-Ray Diffraction Analysis

To evaluate the structural properties of the carbon composite material, the X-ray diffraction method was used to accurately verify its structural properties. The findings from this comprehensive analysis are illustrated in **Figure 2(b).**

The X-ray diffraction (XRD) method is used to evaluate the crystallographic structure of the activated carbon of soybean hulls. The diffractogram indicates two broad peaks around 25 and 43 for $2\theta°$, characteristic of an amorphous structure of soybean carbon [35]-[37]. This result is comparative to XRD analysis result from previous work on activated carbons prepared from plant precursors, showing the absence of crystallization [38]. But, there is difference when this result is compared with the XRD analysis results of activated carbon elaborated from corn cobs by chemical activation with phosphoric acid, which has a crystalline structure [39] [40].

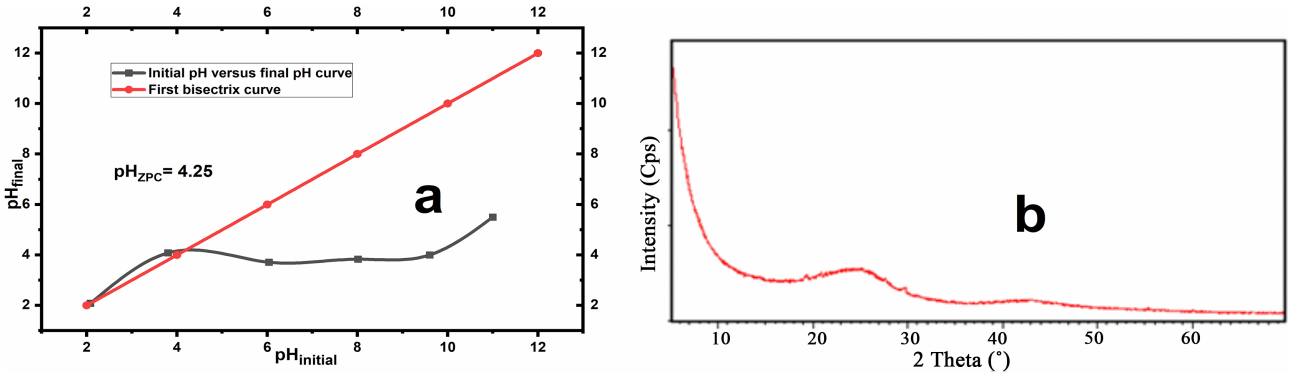

Figure 2. (a) pH at point of zero charge graph, (b) XRD analysis diffractogram.

3.5. Thermogravimetry Analysis

Thermogravimetric and derivative thermogravimetry (DTG) analyses were performed employed thermobalance (NETZSCH TG 209F1). The samples analyzed in alumina crucible. The heating rate was set to 10˚C/min, starting at 30˚C and increasing to 1000˚C in inert atmosphere.

Figure 3 presents the thermogravimetric (TG) and derivative thermogravimetric (DTG) curves for the activated carbon derived from soybean hulls (ASHC). Examination of the thermogravimetric (TG) curve reveals that the initial mass loss of the activated carbon occurs in three main phases as the temperature rises. The first mass loss results from dehydration specifically, the removal of moisture present in the carbon [41]; this loss begins at 25˚C, ends at 140˚C, and accounts for 9.97% of the activated carbon's initial mass. The second mass loss, which is smaller than the first and represents 1.89% of the initial mass, is recorded between 140˚C and 380˚C. This loss may be attributed to the degradation of cellulose and hemicellulose structures [42]. The third mass loss occurs between 380˚C and 890˚C, corresponding to 19.53% of the initial mass of the ASHC. In this temperature range, the mass loss is linked to the elimination of volatile matter and the breakdown of lignin and lignocellulosic structures. In addition, there is fourth mass loss corresponding to 3.93% of initial mass, between 890˚C and 988.8˚C. Furthermore, the residual mass of the analyzed ASHC is 64.68% of the initial mass at 988.8˚C. This demonstrates the thermal stability of the activated carbon derived from soybean hulls and prepared via chemical activation at 400˚C.

The derivative thermogravimetric (DTG) curve shows two endothermic peaks. The first, highly intense endothermic peak at 58.1˚C spanning the range from 22˚C to 150˚C corresponds to the removal of water associated with the ASHC. A second, less intense, broad-based endothermic peak is observed at 657.0˚C, between 550˚C and 800˚C. This can be attributed to decomposition accompanied by a rearrangement of atoms or functional groups on the surface of the ASHC.

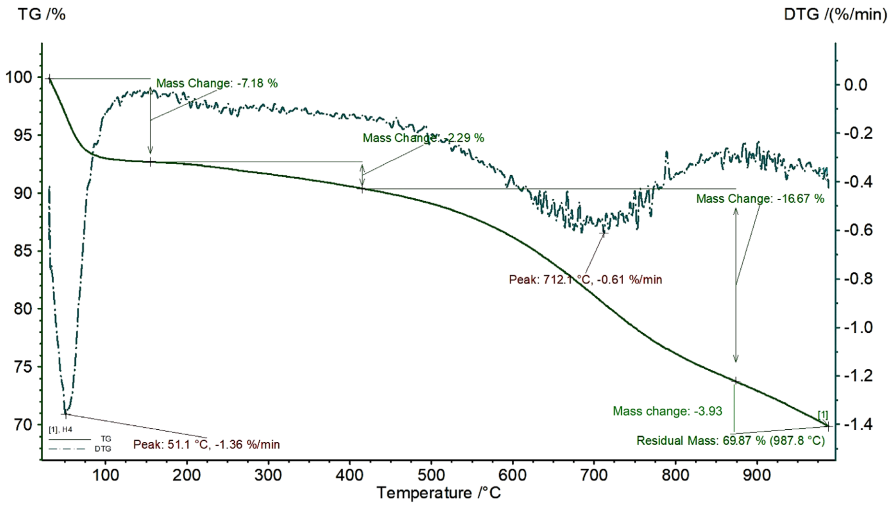

Figure 3. Thermogravimetric (DT-DTG) analysis graph.

3.6. Scanning Electron Microscopy Coupled with Energy-Dispersive X-Rays

Figure 4 shows the scanning electron microscopy image (SEM) of ASHC at 25 µm and the EDX micrograph of the ASHC, while Figure 5 highlights the main chemical elements of ASHC by energy-dispersive X-ray (EDX) analysis.

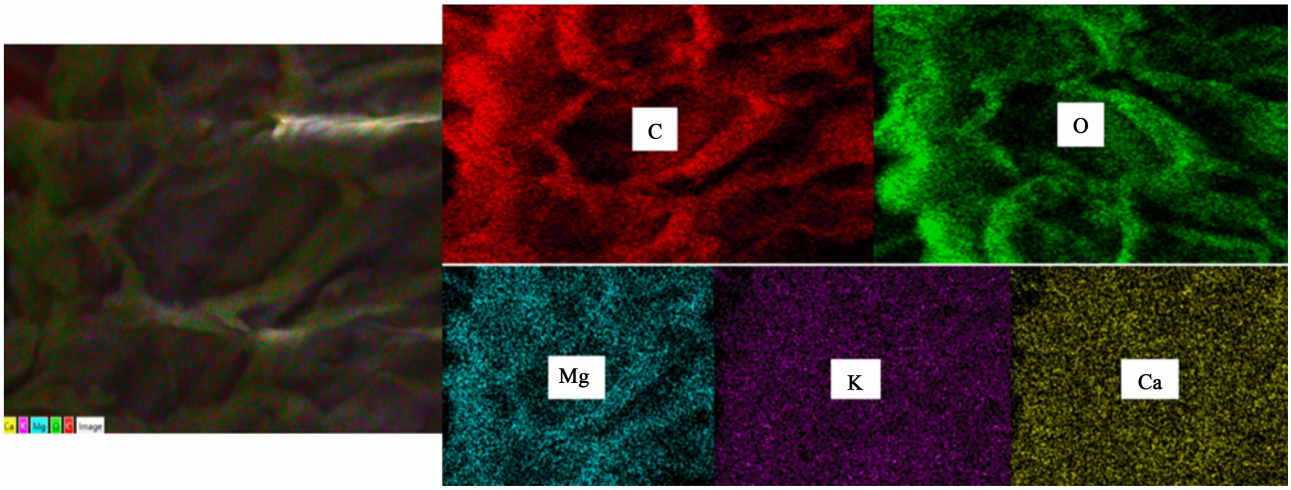

Figure 4. Image of SEM of ASHC.

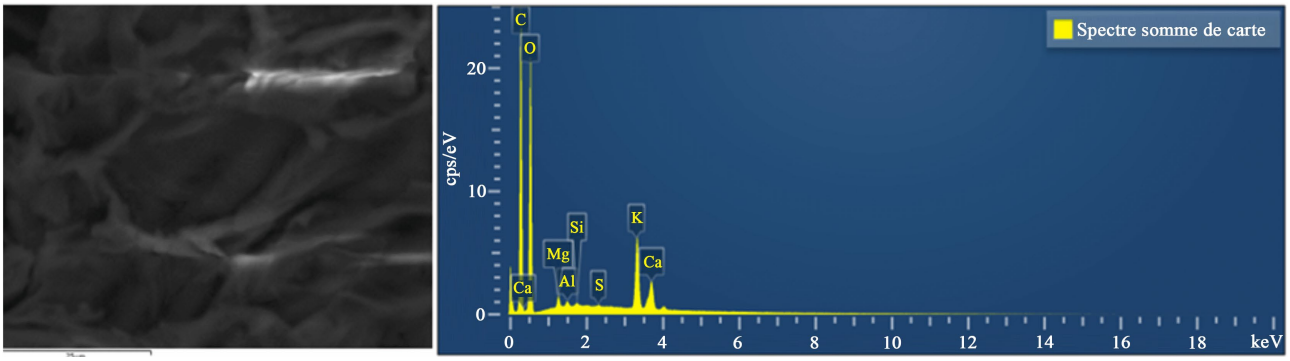

Figure 5. EDX image of ASHC.

Scanning electron microscopy (SEM) technique is used to investigate the morphology of ASHC. An image of SEM shows that the surface of ASHC presents an irregular porosity and amorphous structure; in addition to the pores, particles are present on the surface of the activated carbon. The particles revealed are residues that occurred during the carbonization of plant-based precursors [43]. Therefore, it is observed that the ASHC presents an irregular distribution of pores promoting a heterogeneous surface. The diversity of pores and the presence of cavities in ASHC contribute to promoting the development of adsorption actives sites. Thereby, this can enhance the adsorption capacity of ASHC [44]. The activating agent, phosphoric acid H_3PO_4 and the carbonization processes have played an important role for the porosity development in ASHC. Under the effect of heat, these activating agent molecules, as well as other chemical species, escape from the ma-

terial as a gaseous mixture, subsequently leaving voids or pores [39] [45] [46].

Energy-dispersive X-ray (EDX) spectrum presents the elemental chemical composition of ASHC. Table 1 displays the elemental chemical with their atomic percentage in the analyzed charcoal. It is noted that the ASHC is composed primarily of carbon (58.78%) and oxygen (39.46%), along with trace amounts of other elements such as potassium (0.98%), calcium (0.43%), magnesium (0.23%), aluminum (0.07%), silicon (0.03%), and sulfur (0.02%). Furthermore, the aluminum and silicon originate from impurities and the materials used during the analysis. This chemical composition is consistent with the plant-based origin of the precursor material, namely soybean hulls.

Table 1. Chemical elements content of ASHC.

Element	C	O	Mg	Al	Si	S	K	Ca	Total
% atomic	58.78	39.46	0.23	0.07	0.03	0.02	0.98	0.43	100

3.7. Adsorption Study

3.7.1. Mass Influences of Activated Carbon

Figure 6(a) shows the percentage of MB adsorption per unit mass of ASHC as a function of time at different masses (0.1 g, 0.2 g, 0.3 g and 0.4 g). In this study of mass influences, initial concentration (30 mg·L^{-1}), pH (5.8) of adsorption volume (200 mL) were fixed at ambient temperature (20˚C). It is mainly revealed a correlation between activated carbon dose and dye removal. The maximum percentage of MB adsorbed is reached at a short time as the mass of ASHC increases. The greater the mass of activated carbon used, the faster the adsorption reaction of MB onto ASHC. The number of adsorption sites increases with the mass of the adsorbent. Access to adsorption sites by dye molecules promotes rapid dye removal at shorter times [4].

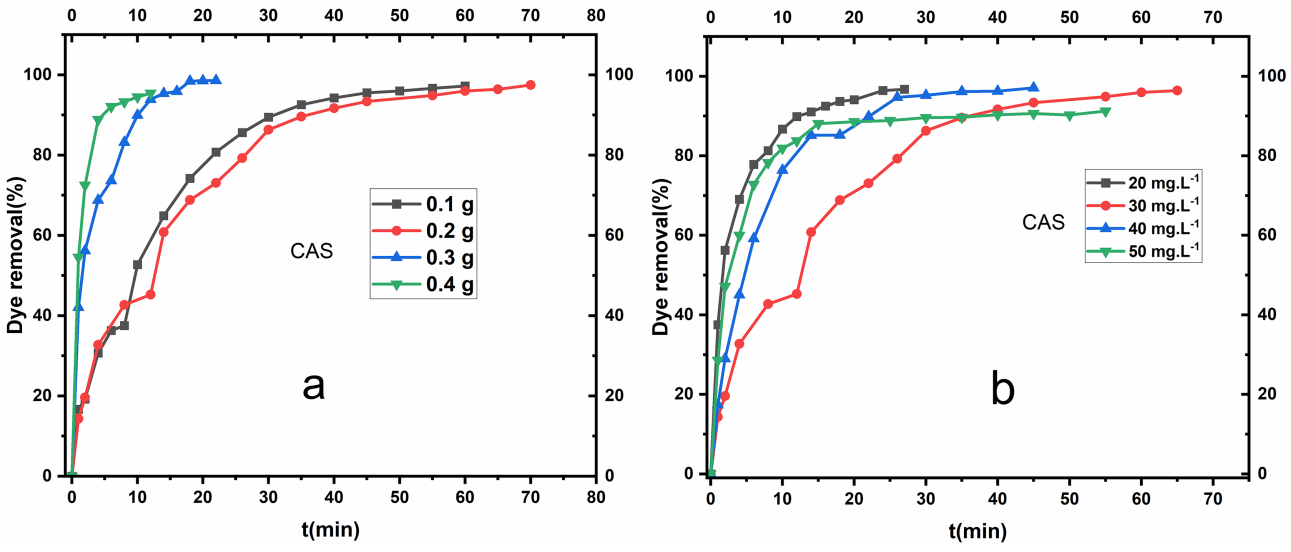

Figure 6. (a) Dosage of ASHC on BM dye (C_0 = 30 mg·L^{-1},) removal, (b) concentration influence on MB dye removal on ASHC (0.2 g); experimental conditions: pH = 5.8; agitation speed: 300 rpm; temperature: 20˚C; adsorption volume: 200 mL.

3.7.2. Influences of Initial Solution Concentrations

Figure 6(b) shows the percentage of MB adsorption per unit mass of ASHC versus time, at different initial MB concentrations C_0 (20 mg·L^{-1}, 30 mg·L^{-1}, 40 mg·L^{-1} and 50 mg·L^{-1}); the adsorbent mass (0.2 g) and the adsorption volume (200 mL) were fixed constant at ambient temperature 20˚C. It ensures that the removal of the MB dye is approximately above 96% after 30 minutes in some conditions (20 mg·L^{-1}, 30 mg·L^{-1}). The maximum rate of removal is highly dependent on the initial concentrations of the solutions. The removal time is shorter for solutions with low initial concentrations than for solutions with high concentrations.

3.7.3. Influence of pH

Figure 7 shows the results of pH influences on the removal of MB from aqueous solutions; the experiment was carried out in conditions where adsorbent mass (0.1 g), initial concentration of MB ($C_0 = 30$ mg·L^{-1}) and adsorption volume (200 mL) were fixed. The initial pH values of various adsorption volumes were separately adjusted from 0 to 10, at ambient temperature (20˚C).

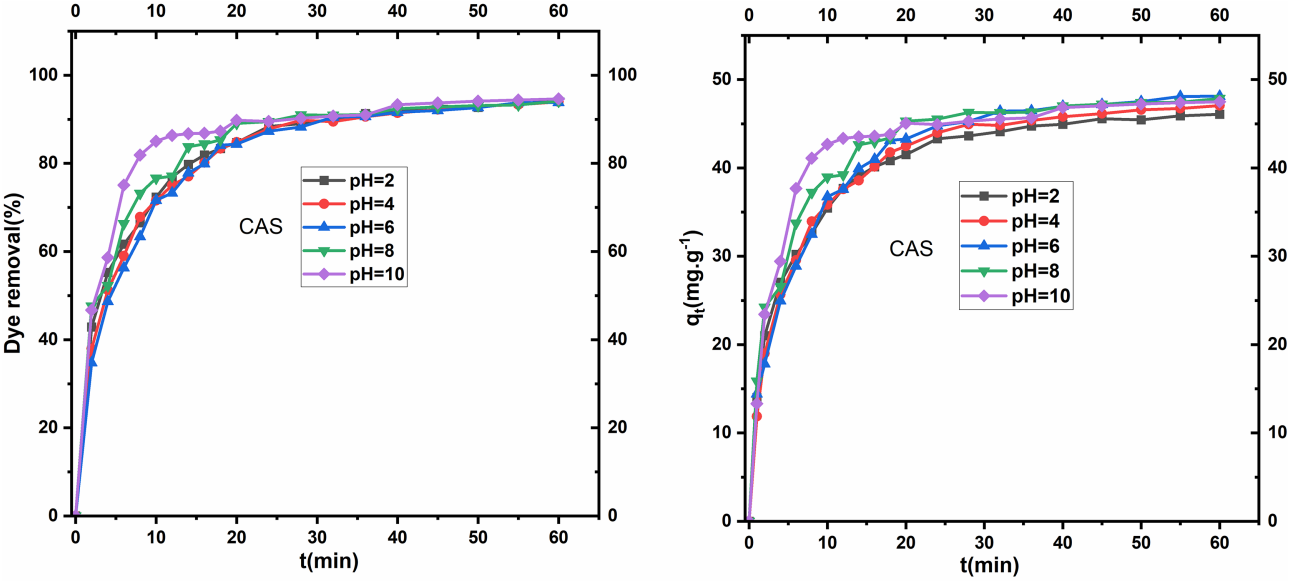

Figure 7. pH influence on MB removal; experimental conditions: adsorbent mass: 0.1 g; agitation speed: 300 rpm; temperature: 20˚C; adsorption volume: 200 mL.

During the first 10 minutes of adsorption, the rate of MB removal increases relatively to the initial pH values (2, 4, 6, 8, 10). However, in the subsequent minutes leading up to adsorption equilibrium, the trend of the curves indicates that the optimal pH for MB removal using ASHC is 10. At higher pH (pH > pH_{ZPC}), the ASHC surface carries a negative charge. This promotes MB removal through electrostatic attraction during the initial minutes of contact (BM + ASHC) [4] [47]. At low pH (pH < pH_{ZPC}), the ASHC surface undergoes protonation and becomes positively charged; this creates competition between H^+ ions and the cationic dye (MB) for adsorption sites and reduces dye removal due to repulsive electrostatic forces. In this

condition, the remarked adsorption can be explained by electrons interactions π-π due to the presence of aromatic rings in both the structure of the dye and the activated carbon derived from soybean hulls (cellulose, hemicellulose, lignin) [48].

The resulting curves show three phases, indicating that MB adsorption occurs in three phases. In the first phase, adsorption is rapid, becomes slow in the second phase, and then approaches equilibrium in the third phase. Since free adsorption sites are available in the first phase, the molecules migrate from the dye to the surface of the carbon and then into the internal pores where they are adsorbed. The number of adsorption sites decreases as the process continues; this would explain the slowness of adsorption until equilibrium is reached.

3.7.4. Adsorption Isotherms, Adsorption Kinetics and Intra-Particle Diffusion

The experimental data were collected in the same conditions for adsorption isotherms as kinetics adsorption and intraparticle diffusion. The average pH of initial solutions concentrations C_0 (20 mg·L^{-1}, 30 mg·L^{-1}, 40 mg·L^{-1}, and 50 mg·L^{-1}) was 5.8; the mass of ASHC applied for adsorption is 0.2 g.

1) Adsorption isotherms

Figure 8 displays the relationship between the quantity of adsorbate molecules per unit of adsorbent mass in an equilibrium phase (q_e) and MB concentration in an equilibrium phase (C_e). The linear curve obtained corresponds to a type C adsorption isotherm in the aqueous phase, according to Giles *et al.* (1974) [49]. This class of isotherm results in linear adsorption, characterised by a constant partition between the solution (adsorbate) and the adsorbent. This implies that the number of available active sites remains constant during adsorption; once adsorbed, the solute molecules cause the gradual opening or activation of new, unused sites. Thus, the number of active sites increases in proportion to the rate of adsorption. The penetration of particles into the micropores proceeds in a regular manner until the pores are filled [49].

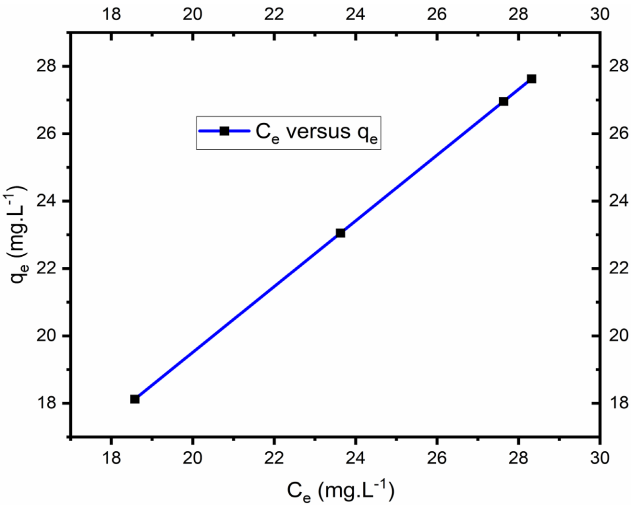

Figure 8. Adsorption isotherm of; experimental conditions: pH = 5.8; adsorbent mass: 0.2 g; agitation speed: 300 rpm; temperature: 20˚C.

Langmuir and Freundlich adsorption isotherms models were applied for the analysis of experimental data of the adsorbent-pollutant system.

Figure 9(a) and Figure 9(b) represent Langmuir and Freundlich models graphs respectively. These graphs are obtained by plotting the linear fit of $\frac{1}{C_e}$ versus $\frac{1}{q_e}$ and $\ln(q_e)$ versus $\ln(C_e)$ successively.

The graph of $\frac{1}{C_e}$ versus $\frac{1}{q_e}$ is linear, with a correlation coefficient R^2 equals 0.998. The experimental data and isotherms parameters are illustrated in Table 2. According to the Langmuir model, separation factor (R_L) determined from data analysis (0.903, 0.861, 0.823, 0.789) is low than for MB solutions (30 mg·L^{-1}, 40 mg·L^{-1}, and 50 mg·L^{-1}). Note that the Langmuir separation factor (R_L) is such that $0 < R_L < 1$. Therefore, the adsorption process of MB on ASHC is favorable. This implies that the adsorption of MB on the ASHC surfaces occurs in a monolayer with a reduction of interactions between molecules [3] [4].

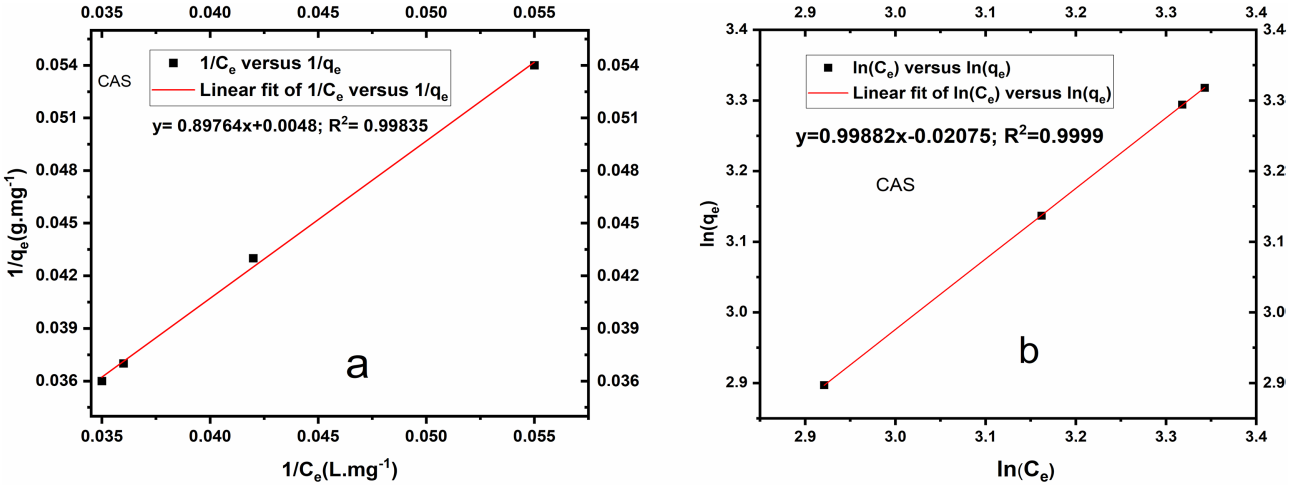

Figure 9. (a) Langmuir adsorption model, (b) Freundlich adsorption model; experimental conditions: pH = 5.8; adsorbent mass: 0.2 g; agitation speed: 300 rpm; temperature: 20˚C.

Table 2. Adsorption isotherm parameters of MB.

Adsorption isotherm	Langmuir isotherm			Freundlich isotherm		
Parameters	q_m (mg·g^{-1})	K_L (g·mg^{-1})	R^2	K_F (g·mg^{-1})	n	R^2
	208.333	0.00534	0.9983	0.9794	1.00118	0.9999

The graph of $\ln(q_e)$ versus $\ln(C_e)$ is linear, with a correlation coefficient R^2 equals 0.999. The constants K_f (0.979) and n (1.001) are both near to 1. The correlation coefficient of the Freundlich model is approximatively equal to the Langmuir model. Therefore, the Freundlich isotherm model describes the adsorption of the MB dye onto the ASHC. This suggests that MB adsorption occurs through the formation of a multilayer structure on a non-homogeneous surface,

with interactions between the molecules constituting the layers. Thereby, both of Langmuir and Freundlich models have tendency to describe equilibrium adsorption data of MB dye on ASHC [50].

2) Adsorption kinetics

Pseudo-first-order and pseudo-second-order adsorption kinetics were applied to analyze the sorption of methylene blue onto activated carbon. Pseudo-first-order adsorption kinetics implies that the reaction rate is proportional to the methylene blue concentration and controlled by surface interactions; furthermore, the adsorption reaction rate increases with the number of available adsorption sites. However, the pseudo-second-order kinetic model assumes a chemical adsorption process with distinct steps.

Figure 10(a) and Figure 10(b) represent pseudo-first-order kinetic and pseudo-second-order kinetic models graphs respectively. These graphs are obtained by plotting the linear fit of $\ln(q_e - q)$ versus t and $\frac{t}{q_t}$ versus t successively.

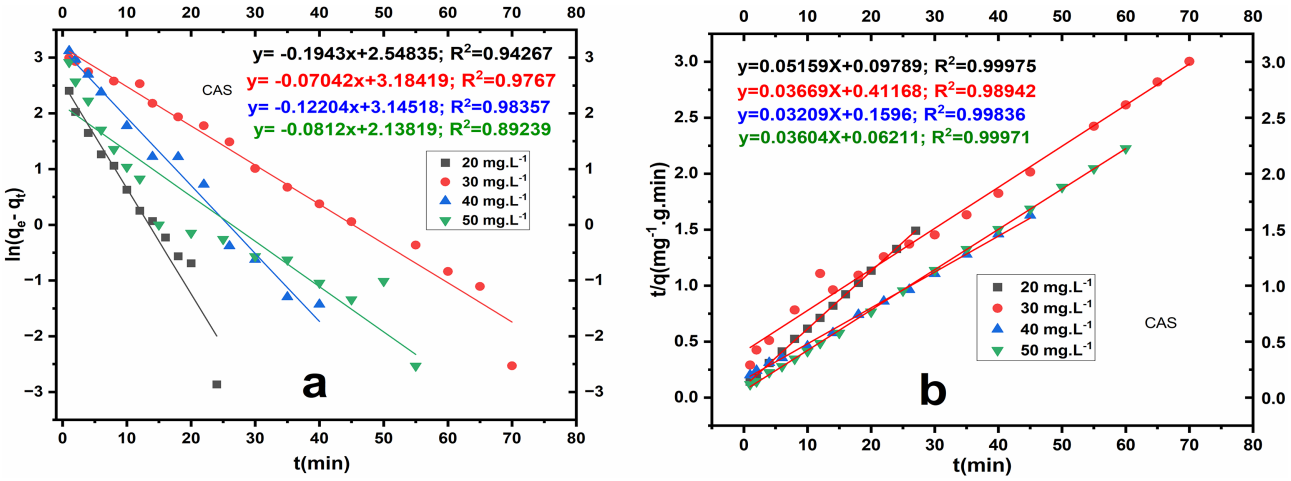

Figure 10. (a) Pseudo-First-Order kinetic, (b) Pseudo-Second-Order kinetic; experimental conditions: Ph = 5.8; adsorbent mass: 0.2 g; agitation speed: 300 rpm; temperature: 20˚C.

The results of the calculations of kinetic models parameters are illustrated in Table 3. The experimental values of the amount of BM adsorbed per unit mass of carbon at equilibrium (18.123, 23.052, 27.628, 26.957 mg·g^{-1}) show a large discrepancy with the amounts of MB adsorbed calculated using pseudo-first-order kinetics (6.927, 8.655, 8.549, 5.812 mg·g^{-1}). This discrepancy implies that there is no correlation between the experimental data and the calculation according to the first-order kinetic model. Consequently, it is deduced that the adsorption of the MB dye by ASHC does not follow the pseudo-first-order kinetic model. The pseudo-first-order kinetic model of adsorption is not suitable for describing the adsorption mechanism of methylene blue on ASHC. Regarding the second-order kinetic model, it should be noted that the results of the calculations of the quantities of BM adsorbed per unit ASHC of coal at equilibrium (19.383; 27.255; 31.162; 27.746 mg·g^{-1}) are approximately equal to the experimental data (18.123, 23.052, 27.628, 26.957 mg·g^{-1}),

mainly at 20 and 50 mg·L^{-1}. The plot of the representative curves $\frac{t}{q_t}$ versus t is linear, and the correlation coefficient value R^2 (0.99) is close to 1, regardless of the initial concentrations of the solutions. Then, it clearly appears that second-order adsorption kinetic model better describes MB dye adsorption on ASHC.

Table 3. Kinetic model parameters of MB adsorption, intraparticle diffusion model parameters.

C_0 (mg·L^{-1})	$q_{e,exp}$ (mg·g^{-1})	Pseudo-First Order kinetic			Pseudo-Second Order kinetic			Intraparticle Diffusion model		
		k_1 (min^{-1})	$q_{e,cal}$ (mg·g^{-1})	R^2	k_2 (mg·g^{-1}·min^{-1})	$q_{e,cal}$ (mg·L^{-1})	R^2	k_d (mg·g^{-1}·min$^{-1/2}$)	C (mg·g^{-1})	R^2
20	18.123	0.194	6.927	0.942	$2.718.10^{-2}$	19.383	0.999	2.359	7.537	0.858
30	23.052	0.070	8.655	0.976	$3.269.10^{-3}$	27.255	0.989	2.952	2.163	0.938
40	27.628	0.122	8.549	0.983	$6.452.10^{-3}$	31.162	0.998	3.863	5.638	0.966
50	26.957	0.081	5.812	0.892	$2.091.10^{-2}$	27.746	0.999	2.122	14.096	0.662

Consequently, the removal of MB dye on ASHC is potentially chemisorption-related; this involves not only valence forces, or electron exchange, but also interactions between the adsorbate molecules and the adsorbent surface [25] [51]. These interactions potentially have facilitated the removal of the MB dye [24].

3) Intraparticle diffusion

The intraparticle diffusion model applied to experimental adsorption data of dye removal is illustrated in Figure 11. This model is determined by plotting the amount of dye adsorbed per mass unit of adsorbent (q_t) versus the square root of time ($t^{\frac{1}{2}}$). The characteristic parameters such as the diffusion rate constant (k_d), the correlation coefficient (R^2), and the diffusion constant (C) have been calculated and are illustrated in Table 2. The values of these parameters are important to interpret the interactions between adsorbate-adsorbent in aqueous phase.

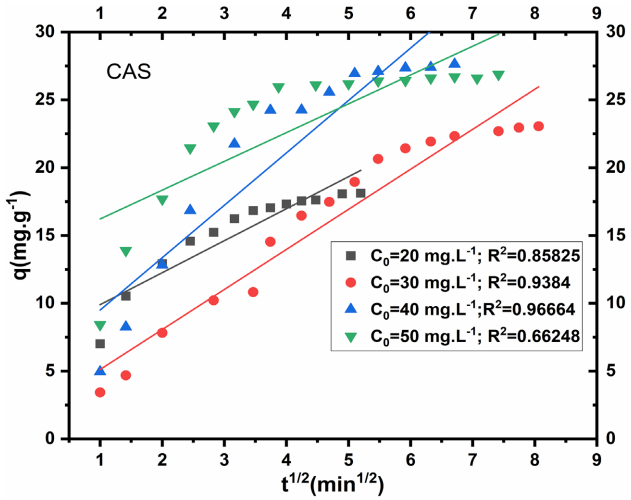

Figure 11. Intraparticle diffusion model of MB adsorption; experimental conditions: pH = 5.8; adsorbent mass: 0.2 g; agitation speed: 300 rpm; temperature: 20˚C.

The diffusion constant being positive implies that the diffusion process to the sites happens quickly and adsorption is rapid [52] [53]. At the initial concentration of 40 mg·L^{-1}, the diffusion coefficient k_d (3.86 mg·g^{-1}·min$^{-1/2}$) is great, the linear correlation coefficient R^2 (0.96) is high, and the corresponding diffusion constant C (5.63 g·mg^{-1}) is positive. Therefore, the diffusion process of MB dye particles into the pores of activated carbon under these conditions happens quickly with rapid adsorption. So, it can be noted that the best condition in which an intraparticle diffusion model better explain the MB adsorption on ASHC is close to 40 mg·L^{-1} [52] [53].

4. Conclusion

This study aimed to remove methylene blue (MB) dye from aqueous solutions using activated soybean hulls carbon elaborated by chemical activation with 50% phosphoric acid. The results of production and characterization of ASHC are interesting, and it was able to remove efficiently MB dye. X-ray diffraction analysis and the low ash content (5.59%) indicate that the activated carbon prepared by chemical activation with phosphoric acid is an amorphous solid. The pH at point of zero charge (pH_{PZC} = 4.25) shows the acidity of ASHC surface. Scanning electron microscopy (SEM) coupled with energy-dispersive X-ray spectroscopy (EDX) illustrates the heterogeneous pore distribution and the elemental chemical composition of the carbons. Indeed, Energy-dispersive X-ray (EDX) analysis of the activated carbon highlights the presence of carbon (58.78%) and oxygen (39.46%). The experimental results reveal that MB dye removal by ASHC exceeds 96%. The pseudo-second-order kinetic model best describes the adsorption of methylene blue by the carbon. Especially, both Langmuir and Freundlich models describe equilibrium adsorption data. The best conditions for intra-particle diffusion are those in which the initial concentration of the solution is close to 40 mg·L^{-1}. The adsorption process is strongly influenced by the pH, concentration of dye and the mass of adsorbent. ASHC is therefore a potential alternative adsorbent for wastewater treatment.

Acknowledgements

The authors are grateful to the directors and all the technicians of laboratories "Laboratoire de Gestion, Traitement et Valorisation des Déchets (GTVD), Laboratoire d'Hydrologie Appliquée et Environnement (LHAE), Université de Lomé, Togo".

Author Contributions

Conceptualization and methodology: Sodoadika Akpolou, Samadou Sanni and Ibrahim Tchakala; investigation: Sodoadika Akpolou, Samadou Sanni, Ibrahim Tchakala and Moursalou Koriko; data curation: Sodoadika Akpolou and Samadou Sanni; writing-review and editing: Sodoadika Akpolou and Samadou Sanni; supervision: Clément Kolawole Balogoun, Ibrahim Tchakala, Moursalou Koriko,

and Gado Tchangbedji. All authors have read and agreed to the published version of the manuscript.

Conflicts of Interest

The authors declare no conflicts of interest that could have influenced the publication of this paper.

References

[1] Abdelhafez, T.F., Radwan, E.K., Sayed, G.H., El Khatib, E.M., Nasr, M.F. and El Gabry, L.K. (2025) Removal of Acid and Basic Dyes from Textile Wastewater Using Modified Acrylic Fibres Waste as an Efficient Adsorbent. *Scientific Reports*, **15**, Article No. 23825. https://doi.org/10.1038/s41598-025-07134-y

[2] Salima, A., Nour, H., Chraka, A., Chtita, S., EL Bouaria, A., Tahirid, M. and Tanane, O. (2025) Methylene Blue Dye Removal Using Activated Carbon Derived from Argan Kernels: Experimental and Computational Studies. *Physical Chemistry Research*, **13**, 365-380.

[3] Baari, M.J., Rudi, L. and Harimu, L. (2025) Adsorption Isotherms, Thermodynamics, and Kinetics of Activated Carbon as Adsorbent to Water Pollutants: A Review. *Chimica Techno Acta*, **12**, Article No. 12214. https://doi.org/10.15826/chimtech.2025.12.2.14

[4] Din, H., Kiran, M., Haq, F., Osman, A.I., Khan, I.A., Aziz, T., *et al*. (2024) Synergizing Date Palm Seeds-Derived Oxidized Activated Carbon: Sustainable Innovation for Enhanced Water Retention, Efficient Wastewater Treatment, and Synthetic Dye Removal. *Chemical Engineering Research and Design*, **204**, 212-227. https://doi.org/10.1016/j.cherd.2024.02.040

[5] Ismail, B.M., Zayed, A.M., Roshdy, M.A., Rafea, M.A. and Mohamed, F.M. (2025) Statistical Modeling of Mutagenic Azo Dye Adsorption on Bagasse Activated Carbon. *Scientific Reports*, **15**, Article No. 20112. https://doi.org/10.1038/s41598-025-04240-9

[6] Aljeboree, A.M., Abdulrazzak, F.H., Saleh, Z.M., Abbas, H.A. and Alkaim, A.F. (2024) Eco-Friendly Adsorption of Cationic (Methylene Blue) and Anionic (Congo Red) Dyes from Aqueous Solutions Using Sawdust. *Engineering Proceedings*, **59**, Article 213. https://doi.org/10.3390/engproc2023059213

[7] Vidovix, T.B., Januário, E.F.D., Cusioli, L.F., Quesada, H.B., Bergamasco, R. and Vieira, A.M.S. (2023) Low-Cost Adsorbent Prepared from Soybean Hulls Residues as Potential Alternative for Cationic Dyes Removal. *Journal of Dispersion Science and Technology*, **44**, 2034-2044. https://doi.org/10.1080/01932691.2022.2059501

[8] Alkhawaja, E.S. and Abdul-Hameed, H.M. (2025) Novel Synthesis and Characterization of Nano-Activated Carbon Derived from Agricultural Orange Peel Waste. *International Journal of Design & Nature and Ecodynamics*, **20**, 31-41. https://doi.org/10.18280/ijdne.200104

[9] Kaga, T.T., Segbeaya, K.N., Pallier, V. and Feuillade, G. (2024) Synthesis and Characterization of Activated Carbons from Avocado Kernel; Application to Phenol Removal. *American Journal of Materials Science and Engineering*, **12**, 1-12.

[10] Balogoun, C., Bawa, M., Osseni, S. and Aina, M. (2015) Préparation des charbons actifs par voie chimique à l'acide phosphorique à base de coque de noix de coco. *International Journal of Biological and Chemical Sciences*, **9**, Article 563. https://doi.org/10.4314/ijbcs.v9i1.48

[11] Faouzou, O., Amenuvevega, D.A., Ibrahim, T., Samadou, S., Tomkouani, K., Seyf-Laye, A.M., *et al*. (2024) Synthesis of Activated Carbon from Cassava Peeling and Its Applications for Removal of Methylene Blue. *American Journal of Physical Chemistry*, **13**, 9-16. https://doi.org/10.11648/j.ajpc.20241301.12

[12] Tchakala, I., Bawa, L., Djaneye-Boundjou, G., Doni, K. and Nambo, P. (2012) Optimisation du procédé de préparation des charbons actifs par voie chimique (H_3PO_4) à partir des tourteaux de Karité et des tourteaux de Coton. *International Journal of Biological and Chemical Sciences*, **6**, 461-478. https://doi.org/10.4314/ijbcs.v6i1.42

[13] Armand, A.E., Augustin, Y.Y., Urbain, K.Y. and Albert, T. (2020) Optimisation de la préparation de charbons activés à base d'épis de maïs et caractérisation physi-co-chimique. *International Journal of Innovation and Applied Studies*, **29**, 1161-1171. http://www.ijias.issr-journals.org/

[14] Kumaravel, S., Geetha, M., Niyitanga, T., Kumar, D.S., Al-Ansari, M.M., Mythili, R., *et al*. (2024) Preparation and Characterization of Activated Carbon from Corn Cob by Chemical Activation and Their Adsorption of Brilliant Green Dye from Wastewater. *Process Safety and Environmental Protection*, **188**, 1338-1345. https://doi.org/10.1016/j.psep.2024.05.127

[15] Diallo, A.D., Diakite, S. and Diallo, A.S. (2022) Production et caractérisation d'un charbon actif à base de coques d'arachide suivie d'un test de dépollution d'eaux usées avec le charbon actif en poudre, CAP. *Afrique Science*, **21**, 57-70. http://www.afriquescience.net/article.php?nid=276&&code=Vol.21,%20N%C2%B05%20(2022)&id=6

[16] Evwierhoma, E.T., Madubiko, O.D. and Jaiyeola, A. (2018) Preparation and Characterization of Activated Carbon from Bean Husk. *Nigerian Journal of Technology*, **37**, Article 674. https://doi.org/10.4314/njt.v37i3.17

[17] Saleem, J., Moghal, Z.K.B., Tahir, F., Al-Ansari, T. and McKay, G. (2025) Environmental Impacts and Adsorption Isotherms of Coconut Shell Activated Carbon: Effect of Acid Activation, Water, and Fuel. *C*, **11**, Article 22. https://doi.org/10.3390/c11010022

[18] Shamsuddin, M.S., Yusoff, N.R.N. and Sulaiman, M.A. (2016) Synthesis and Characterization of Activated Carbon Produced from Kenaf Core Fiber Using H3PO4 Activation. *Procedia Chemistry*, **19**, 558-565. https://doi.org/10.1016/j.proche.2016.03.053

[19] Siragi D B, M., Natatou, I. and Dubois, V. (2025) Synthesis of Activated Carbon from *Balanites aegyptiaca* and *Hyphaene thebaica* Shells by Physical Activation. *Carbon Trends*, **21**, Article 100555. https://doi.org/10.1016/j.cartre.2025.100555

[20] Zayed, A.M., Metwally, B.S., Masoud, M.A., Mubarak, M.F., Shendy, H., Petrounias, P., *et al*. (2023) Facile Synthesis of Eco-Friendly Activated Carbon from Leaves of Sugar Beet Waste as a Superior Nonconventional Adsorbent for Anionic and Cationic Dyes from Aqueous Solutions. *Arabian Journal of Chemistry*, **16**, Article 104900. https://doi.org/10.1016/j.arabjc.2023.104900

[21] Belyea, R.L., Steevens, B.J., Restrepo, R.J. and Clubb, A.P. (1989) Variation in Composition of By-Product Feeds. *Journal of Dairy Science*, **72**, 2339-2345. https://doi.org/10.3168/jds.s0022-0302(89)79366-8

[22] Fitri Faradilla, R.H., Lucia, L. and Hakovirta, M. (2021) Hydrothermal Carbonization of Soybean Hulls for the Generation of Hydrochar: A Promising Valorization Pathway for Low Value Biomass. *Environmental Nanotechnology, Monitoring & Management*, **16**, Article 100571. https://doi.org/10.1016/j.enmm.2021.100571

[23] Atheba, P., Gbassi, G.K., Dongui, B., Bamba, D., Yolou, S. and Trokourey, A. (2014)

Études de la porosité, de la surface spécifique et des fonctions de surface de charbons actifs préparés après carbonisation artisanale des coques de noix de coco. *Les Tech-Nologies de Laboratoire*, **8**, 126-136.

[24] Akpolou, S., Sanni, S., Zaneidou, Y., Tchakala, I., Koriko, M. and Tchangbedji, G. (2026) Synthesis and Characterization of Activated Carbon from Bean Pods: Adsorption Kinetics of Methylene Blue Dye, Adsorption Isotherms and Intra-Particle Diffusion. *Journal of Materials and Environmental Science*, **17**, 326-344. http://www.jmaterenvironsci.com/Document/vol17/vol17_N2/JMES-2026-1702017-Akpolou.pdf

[25] Medhat, A., El-Maghrabi, H.H., Abdelghany, A., Abdel Menem, N.M., Raynaud, P., Moustafa, Y.M., *et al*. (2021) Efficiently Activated Carbons from Corn Cob for Methylene Blue Adsorption. *Applied Surface Science Advances*, **3**, Article 100037. https://doi.org/10.1016/j.apsadv.2020.100037

[26] Bortoluz, J., Ferrarini, F., Bonetto, L.R., da Silva Crespo, J. and Giovanela, M. (2020) Use of Low-Cost Natural Waste from the Furniture Industry for the Removal of Methylene Blue by Adsorption: Isotherms, Kinetics and Thermodynamics. *Cellulose*, **27**, 6445-6466. https://doi.org/10.1007/s10570-020-03254-y

[27] Abdel-Aziz, A.B., Alrefaey, K.A., El-Taweel, R.M., Sh, H., Pal, K., Fahim, I.S., *et al*. (2023) Bio-Inspired Adsorption Sheets from Waste Material for Anionic Methyl Orange Dye Removal. *SN Applied Sciences*, **5**, Article No. 371. https://doi.org/10.1007/s42452-023-05600-8

[28] Bassareh, H., Karamzadeh, M. and Movahedirad, S. (2023) Synthesis and Characterization of Cost-Effective and High-Efficiency Biochar for the Adsorption of Pb^{2+} from Wastewater. *Scientific Reports*, **13**, Article No. 15608. https://doi.org/10.1038/s41598-023-42918-0

[29] Brou Guillaume, K., Serpokrylov, N.S., Smolyanichenko, A.S., Cheblakova, E.G., Gorina, V.A. and Yoboué, D.V. (2019) Physico-Chemical Characteristics of the Char from Cashew Nuts Shells and Activated Carbons Obtained from It. *Environnement, Ingénierie & Développement*, **82**, Article No. 7728. https://doi.org/10.4267/dechets-sciences-techniques.4164

[30] Maazou, S.D.B., Hima, H.I., Malam Alma, M.M., Adamou, Z. and Natatou, I. (2018) Elimination du chrome par du charbon actif élaboré et caractérisé à partir de la coque du noyau de *Balanites aegyptiaca*. *International Journal of Biological and Chemical Sciences*, **11**, Article 3050. https://doi.org/10.4314/ijbcs.v11i6.39

[31] Mamane, O.S., Boukari, M.S.D. and Chaibou, A.R. (2018) Valorisation de coques de noix de *Balanites aegyptiaca* (L.) del. et élimination du Chrome en solution. *Afrique Science*, **14**, 167-181. https://www.researchgate.net/publication/332259201_Valorisation_de_coques_de_noix_de_Balanites_aegyptiaca_L_Del_et_elimination_du_Chrome_en_solution

[32] Ouedrhiri, M., Jaaouan, K., Mohtadi, F.E., Benismail, C. and Begdouri, A.A. (2018) Charbons actifs à partir des coques d'olives (Picholine marocaine): Préparation, caractérisation et évaluation de leur capacité de dépollution des margines. *Revue Marocaine des Sciences Agronomiques et Vétérinaires*, **6**, 362-373.

[33] Usman, A., Ibrahim, M. and Bishi, U. (2025) Adsorption of Dyes from Synthetic Wastewater Using Doum Palm Activated Carbon. *South African Journal of Chemistry*, **79**, 10-17. https://doi.org/10.17159/0379-4350/2025/v79a02

[34] Yunusa, U., Abdullahi, Y., Garba, M., Bello, G.N., Aji, M.A. and Kubo, A.I. (2021) Selective and Simultaneous Removal of Methylene Blue and Cadmium (II) from Wastewater Using Waste Biomass Derived Porous Carbon. *Journal of Materials and*

Environmental Science, **12**, 1243-1258.
http://www.jmaterenvironsci.com/Document/vol12/vol12_N9/JMES-2021-12100-Yunusa.pdf

[35] Suyoga Wiguna, A.A.G., Mardana, I.B.P. and Artawan, P. (2024) Synthesis and Characterization of Activated Carbon Prepared from Rice Husk by Physics-Chemical Activation. *Indonesian Physical Review*, **7**, 281-290. https://doi.org/10.29303/ipr.v7i2.311

[36] Touzani, I., El Machrafi, I., Harboul, K., Boudouch, O., Alouiz, I., Hammani, K., *et al*. (2024) Evaluation of Activated Carbons Prepared from Bioprecursors for the Removal of Cadmium and Chromium (VI). *Applied and Environmental Soil Science*, **2024**, 1-11. https://doi.org/10.1155/2024/8663114

[37] Salim, A., El Bouari, A., Chraka, A., Chtita, S., Tahiri, M. and Tanane, O. (2025) Integrated Experimental and Computational Investigation of Methylene Blue Adsorption on Activated Carbon. *International Journal of Energy and Water Resources*, **9**, 2475-2489. https://doi.org/10.1007/s42108-025-00401-8

[38] Zięzio, M., Charmas, B., Jedynak, K., Hawryluk, M. and Kucio, K. (2020) Preparation and Characterization of Activated Carbons Obtained from the Waste Materials Impregnated with Phosphoric Acid(V). *Applied Nanoscience*, **10**, 4703-4716. https://doi.org/10.1007/s13204-020-01419-6

[39] Olorundare, O.F., Msagati, T.A.M., Krause, R.W.M., Okonkwo, J.O. and Mamba, B.B. (2014) Activated Carbon from Lignocellulosic Waste Residues: Effect of Activating Agent on Porosity Characteristics and Use as Adsorbents for Organic Species. *Water, Air, & Soil Pollution*, **225**, Article No. 1876. https://doi.org/10.1007/s11270-014-1876-2

[40] Farma, R. (2019) Physical Properties Analysis of Activated Carbon from Oil Palm Empty Fruit Bunch Fiber on Methylene Blue Adsorption. *Journal of Technomaterials Physics*, **1**, 67-73. https://doi.org/10.32734/jotp.v1i1.824

[41] Zanella, O., Bilibio, D. and Priamo, W.L. (2025) Porous Structure and Characterization of Activated Carbons from the Grape Stalks. *Sustainable Processes Connect*, **1**, Article 1. https://doi.org/10.69709/susproc.2025.138473

[42] Sanni, S., Tchakala, I., Kodom, T., Karamoko, B.A., Bawa, L.M. and Holade, Y. (2025) Activated Carbons Derived from Brewing Cereal Residues and Pineapple Peelings for Removal of Acid Orange 7 (AO7) Dye. *Molecules*, **30**, Article 881. https://doi.org/10.3390/molecules30040881

[43] Hazourli, S., Ziati, M., Hazourli, A. and Cherifi, M. (2007) Valorisation d'un résidu naturel ligno-cellulosique en charbon actif—exemple des noyaux de dattes. *Revue des Energies Renouvelables*, 187-192.

[44] Amari, A., Noreen, A., Osman, H., Sammen, S.S., Al-Ansari, N. and Salman, H.M. (2023) Investigation of the Viable Role of Oil Sludge-Derived Activated Carbon for Oily Wastewater Remediation. *Frontiers in Environmental Science*, **11**, Article ID: 1138308. https://doi.org/10.3389/fenvs.2023.1138308

[45] Fathy, N.A., Sayed Ahmed, S.A. and Abo El-Enin, R.M.M. (2012) Effect of Activation Temperature on Textural and Adsorptive Properties for Activated Carbon Derived from Local Reed Biomass: Removal of P-Nitrophenol. *Environmental Research, Engineering and Management*, **59**, 10-22. https://doi.org/10.5755/j01.erem.59.1.961

[46] Semmache, N., Miloudi, A., Kiari, M., Nair, S., Youcef, B., Alharthi, S., *et al*. (2026) Preparation, Characterization, and Adsorptive Capacity of Powdered Activated Carbon Based on *Opuntia Ficus Indica* Seeds Cakes. *Open Chemistry*, **24**, Article 20250253. https://doi.org/10.1515/chem-2025-0253

[47] Ramutshatsha-Makhwedzha, D., Mavhungu, A., Moropeng, M.L. and Mbaya, R. (2022) Activated Carbon Derived from Waste Orange and Lemon Peels for the Adsorption of Methyl Orange and Methylene Blue Dyes from Wastewater. *Heliyon*, **8**, e09930. https://doi.org/10.1016/j.heliyon.2022.e09930

[48] Ederer, J., Ecorchard, P., Slušná, M.Š., Tolasz, J., Smržová, D., Lupínková, S., *et al*. (2022) A Study of Methylene Blue Dye Interaction and Adsorption by Monolayer Graphene Oxide. *Adsorption Science & Technology*, **2022**, Article 7385541. https://doi.org/10.1155/2022/7385541

[49] Giles, C.H., Smith, D. and Huitson, A. (1974) A General Treatment and Classification of the Solute Adsorption Isotherm. I. Theoretical. *Journal of Colloid and Interface Science*, **47**, 755-765. https://doi.org/10.1016/0021-9797(74)90252-5

[50] Menezes, A., Goveas, L.C., Vinayagam, R. and Selvaraj, R. (2025) Harnessing Carbon-Based Adsorbents for Poly- and Perfluorinated Substance Removal: A Comprehensive Review. *Journal of Water Process Engineering*, **69**, Article 106621. https://doi.org/10.1016/j.jwpe.2024.106621

[51] Bayça, F. (2026) Molecular Adsorption Mechanism of Methylene Blue Dye on Ulexite. *Scientific Reports*, **16**, Article No. 9749. https://doi.org/10.1038/s41598-026-40340-w

[52] Mohamed Nasser, S., Abbas, M. and Trari, M. (2024) Understanding the Rate-Limiting Step Adsorption Kinetics onto Biomaterials for Mechanism Adsorption Control. *Progress in Reaction Kinetics and Mechanism*, **49**, 1-26.

[53] Vashishtha, M. and Kumar, K.V. (2026) Insights into Solid-Liquid Adsorption Kinetics: Theory, Mechanisms, and Practical Guidelines. *ACS ES&T Water*, **6**, 2569-2601. https://doi.org/10.1021/acsestwater.5c00497